J Shoulder Elbow Surg (2019) 28, 1886–1896

ELSEVIER

Journal of Shoulder and Elbow Surgery

www.elsevier.com/locate/ymse

Bone adaptation impact of stemless shoulder implants: a computational analysis

Manuel Comenda, MEng[a], Carlos Quental, PhD[a,*], João Folgado, PhD[a], Marco Sarmento, MD[b], Jacinto Monteiro, PhD, MD[b]

[a]*IDMEC, Instituto Superior Técnico, Universidade de Lisboa, Lisbon, Portugal*
[b]*Faculty of Medicine, Universidade de Lisboa, Lisbon, Portugal*

Background: Despite stemless implants showing promising functional and radiologic clinical outcomes, concerning signs of complications, such as bone resorption, have been reported. The aim of this study was to investigate the influence of 5 stemless designs on the bone adaptation process of the humerus.
Methods: Three-dimensional finite element models of shoulder arthroplasties were developed considering stemless designs based on the Eclipse, Global Icon, SMR, Simpliciti, and Sidus stemless systems. For the designs not possessing a collar that covers the entire resected surface of the humerus, conditions of contact and no contact were simulated between the humeral head components and the bone surface. By use of a bone remodeling model, computational simulations were performed considering 6 load cases of standard shoulder movements. The bone adaptation process was evaluated by comparing differences in bone density between the implanted models and the intact model of the humerus.
Results: Overall, the design of the stemless implants had a relevant impact on the bone adaptation process of the humerus. The Eclipse-based design caused the largest bone mass loss, whereas the SMR-based design caused the least. When contact was simulated between the humeral head components of the SMR-, Simpliciti-, and Sidus-based designs and the resected bone surface, bone resorption increased.
Discussion: Considering only the bone adaptation process, the results suggest that the SMR-based implant presents the best performance and that contact between the humeral head component and the resected bone surface should be avoided. However, because other factors must be considered, further investigation is necessary to allow definite recommendations.
Level of evidence: Basic Science Study; Computer Modeling

Keywords: Shoulder joint; shoulder arthroplasty; stemless implants; bone adaptation; stress shielding; finite element method

Annual incidence rates of shoulder arthroplasty have nearly tripled over the past decade.[23] Yet, even though shoulder arthroplasty is regarded as a reliable treatment for rheumatoid and osteoarthritic glenohumeral joints, its long-term performance is still associated with several complications. The stress shielding effect, characterized by a negative adaptation of bone due to changes in load, is often considered a key contributing factor to some of the

Institutional review board/ethical committee approval was not required for this basic science study.

*Reprint requests: Carlos Quental, PhD, IDMEC, Instituto Superior Técnico, Universidade de Lisboa, Av Rovisco Pais, 1 1049-001 Lisboa, Portugal.

E-mail address: carlos.quental@tecnico.ulisboa.pt (C. Quental).

1058-2746/$ - see front matter
https://doi.org/10.1016/j.jse.2019.03.007

shoulder arthroplasty complications.[26,32] The negative remodeling processes weaken the bone, making it either thinner or more porous, which increases the risk of implant failure and periprosthetic fractures.[22]

To avoid stem-related complications and reduce the occurrence of stress shielding, there is currently a trend to shorten the stem length in humeral components. By relying on a metaphyseal fixation using a standard humeral neck cut, the last generation of shoulder implants, called ''stemless implants,'' preserves more bone stock than standard humeral components, which is critical for future revision surgery, especially considering the increase in a younger population needing surgery[24]; eliminates diaphyseal stress concentrations; and allows an easier revision surgical procedure.[2,16]

Clinical studies addressing the performance of stemless implants have shown promising functional and radiologic clinical outcomes, comparable with those of standard stemmed implants, at short-term, midterm, and long-term follow-up.[15] Nonetheless, despite the limited number of reports, there is evidence of the prevalence of complications that raise concern. In a prospective study including 78 patients treated with the Eclipse Stemless Shoulder Prosthesis (Arthrex, Karlsfeld, Germany), Habermeyer et al[13] observed a lowering of the density of cancellous bone in the proximal humerus in 41.3% of patients at a mean radiologic follow-up of 72 months. Considering only anatomic stemless shoulder replacements using the Eclipse prosthesis, Hawi et al[15] clinically and radiologically monitored 43 patients in a prospective cohort study for a mean of 9 years and observed a lowering of bone mineral density in the superior proximal region of the humerus on the anteroposterior radiographs of 29.4% of patients. Heuberer et al[18] also identified internal stress shielding, defined as reduced bone mineral density around the hollow screw, on 5-year postoperative radiographs of 42.5% of patients in a prospective evaluation of 73 consecutive shoulders treated with the Eclipse prosthesis. Recently, in a prospective, nonrandomized, multicenter study including 9 European centers, lower bone density or atrophy around the humeral component was noted radiologically, at a mean follow-up of 48 months, in 4 of 105 patients treated with the Sidus Stem-Free Shoulder System (Zimmer Biomet, Warsaw, IN, USA).[20] It is worth noting that, unlike stemmed implants, whose designs were considered similar enough not to cause drastic differences in performance, the stemless implant designs available for use have significant differences, which prevent the extrapolation of findings from 1 specific design to all stemless designs.[2] Hence, considering the limited knowledge on stemless implants, further investigation is necessary to gain further insight into their long-term performance.

Computational studies focusing on stemless implants are scarce. Razfar et al[31] evaluated the effect of the humeral component length on the stresses in the proximal humerus based on 3-dimensional (3D) finite element analyses. The application of shorter stems was found to raise trabecular bone stresses in the proximal head above those in the intact bone, suggesting less potential for stress shielding. Considering several generic stemless implants with central, peripheral, and boundary-crossing fixation features, Reeves et al[32] studied the effect of implant geometry on the simulated stress and strain response of the proximal humerus. The centrally pegged implants were reported to present the least bone volume percentage expected to resorb. In a study comparing the bone adaptation process of the humerus owing to a resurfacing implant based on the Global CAP system (DePuy, Warsaw, IN, USA) and a stemless implant based on the Sidus Stem-Free System, Santos et al[33] observed less bone density loss at the fixation site of the stemless implant. To our knowledge, the bone adaptation process of the humerus due to different stemless implants has not been addressed. The aim of this study was to evaluate the influence of different stemless designs, available for use, on the bone adaptation process of the humerus using 3D finite element models.

Methods

Finite element model

A 3D model of the right humerus was reconstructed from the Visible Human Male data set[36] using ITK-SNAP.[38] Considering the variability in implant designs, 5 stemless implants were modeled based on the Eclipse Stemless Shoulder Prosthesis, Global Icon Stemless Shoulder System (DePuy), SMR Stemless (LimaCorporate, San Daniele del Friuli, Italy), Simpliciti Shoulder System (Tornier, Edina, MN, USA), and Sidus Stem-Free Shoulder System. For the sake of simplicity, these implants are referred to hereafter as ''Eclipse-based,'' ''Global Icon–based,'' ''SMR-based,'' ''Simpliciti-based,'' and ''Sidus-based'' models, respectively. The shoulder arthroplasties, depicted in Figure 1, were virtually simulated in the SolidWorks program (Dassault Systèmes, Waltham, MA, USA), following the surgical guidelines available for each implant, to mimic the actual procedures as closely as possible. The sizes of the implants were selected to fit the humerus under analysis according to the recommendations of the manufacturers and orthopedic surgeons.

From the 3D geometric models created, 6 finite element models were developed in the Abaqus 2017 program (Dassault Systèmes) considering an intact model of the humerus, prior to shoulder arthroplasty, and 5 implanted models. A sensitivity analysis was performed to define the density of the finite element meshes using linear tetrahedral (C3D4) elements. All components of the stemless implants were modeled as linear elastic, homogeneous, and isotropic materials. The heads, made of a cobalt-chromium alloy, were assigned a Young's modulus of 230 GPa and a Poisson's ratio of 0.3, whereas the metaphyseal components, made of a titanium alloy, were assigned a Young's modulus of 115 GPa and a Poisson's ratio of 0.3. The material properties of bone result from the bone remodeling model applied assuming a Young's modulus of 17.5 GPa for cortical bone.[12,26,33]

The interactions between bone and the coated or blasted regions of the different metaphyseal components were modeled considering 2 alternative conditions: a fully completed condition

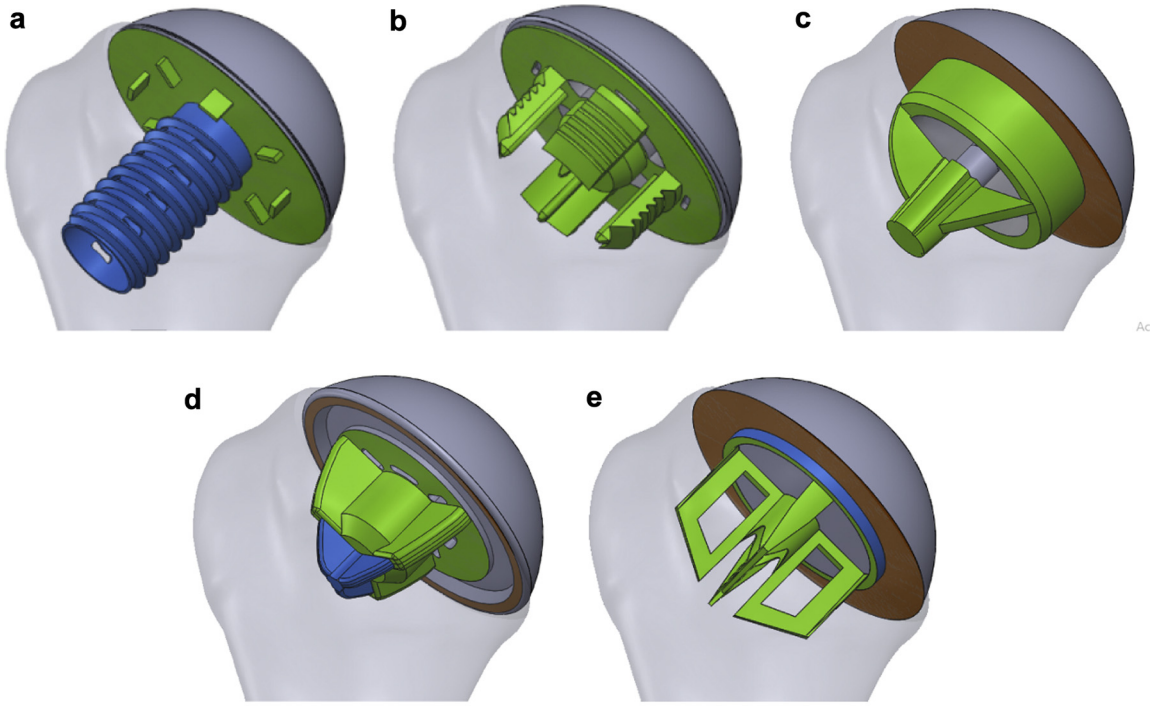

Figure 1 Three-dimensional geometric models of shoulder arthroplasty considering Eclipse-based **(a)**, Global Icon–based **(b)**, SMR-based **(c)**, Simpliciti-based **(d)**, and Sidus-based **(e)** stemless implants. The *green* and *blue* regions represent bonded and contact interactions, respectively. The *brown* regions represent the interaction surfaces of the humeral head components of the SMR-, Simpliciti-, and Sidus-based implants when contact is simulated with the surface of the resected humerus.

of osseointegration, for which full osseointegration occurred, and a fully absent condition of osseointegration, for which no osseointegration occurred.[14,33,37] For the fully completed condition, a tie constraint was used to define the interactions between bone and the coated or blasted surfaces, highlighted in green in Figure 1. For the fully absent condition, a surface-to-surface contact formulation was considered. The interactions of non-coated and nonblasted surfaces with bone were always described by a surface-to-surface contact formulation, as illustrated in Figure 1. According to the surgical techniques, the humeral heads of the SMR and Sidus implants sit flush on the resected humerus whereas the head of the Simpliciti implant does not. Yet, because less-than-perfect placement can occasionally be achieved, both placement conditions were considered, that is, different simulations were performed considering contact and no contact between the humeral heads of the SMR-, Sidus-, and Simpliciti-based implants and the resected surface of bone. Contact at these implant surfaces, represented in brown in Figure 1, allows loads to be transferred to the bone through these interfaces. It should be noted that the humeral heads of the Eclipse-based and Global Icon–based implants do not contact the bone because their metaphyseal components possess a collar that covers the entire resected surface. Table I summarizes the friction coefficients considered for the different contact interactions.[5,10,21,30,35]

Table I Friction coefficients considered for contact interactions between bone and different components of stemless implants

Interaction	Friction coefficient
Bone and titanium plasma spray (Eclipse trunion)	0.60
Bone and trabecular titanium (SMR core)	2.20
Bone and sintered titanium beads (Simpliciti nucleus)	0.53
Bone and rough titanium coating (Sidus anchor, Global Icon anchor)	0.60
Bone and cobalt-chromium	0.26
Bone and titanium	0.36

Bone remodeling model

The bone remodeling model used is a node-based approach to the computational model developed by Fernandes et al,[8] which describes bone as a cellular material with a microstructure obtained through the periodic repetition of cubic unit cells with rectangular holes.[26,28] For each point, bone is characterized by the dimensions (**a**) of the rectangular holes, which control bone density (μ), and the angles (**θ**), which control the material orientation. The bone remodeling process is formulated as a balance between the structural stiffness and a biological term related to the cost of bone maintenance. Mathematically, it is given by the following:

$$\sum_{P=1}^{NC}\left[\alpha^{p}\frac{\partial E^{H}_{ijkl}}{\partial \mathbf{a}}\varepsilon_{ij}\varepsilon_{kl}\right]-k\,\frac{\partial(\mu^{m})}{\partial \mathbf{a}}=0 \qquad (1)$$

$$\sum_{P=1}^{NC}\left[\alpha^{P}\frac{\partial E^{H}_{ijkl}}{\partial \boldsymbol{\theta}}\varepsilon_{ij}\varepsilon_{kl}\right]=0 \qquad (2)$$

in which NC is the number of applied load conditions and α^P are load weight factors satisfying $\sum_{P=1}^{NC}\alpha^{P}=1$. In brief, the bone adaptation process is simulated by computing the homogenized material properties (E^H_{ijkl}) of bone using the homogenization method described by Guedes and Kikuchi.[11] The material properties are provided to the finite element code, which computes the strain field ($\boldsymbol{\varepsilon}$) that is used to update $\mathbf{a}$ and $\boldsymbol{\theta}$ according to Equations 1 and 2, respectively. These steps are repeated in an iterative procedure until bone is in equilibrium, that is, until the conditions expressed in Equations 1 and 2 are satisfied. The parameters κ and m are bone remodeling parameters that define the cost of bone maintenance.

Six load cases, related to 10°, 60°, and 90° arm positions of abduction in the frontal plane and anterior flexion in the sagittal plane, were applied. Considering the relative frequencies of arm movements during daily activities, the weight factors (α^P) for the 10°, 60°, and 90° positions were 0.25, 0.06, and 0.01, respectively, for abduction and 0.54, 0.12, and 0.02, respectively, for flexion.[3,4] Each load case included the glenohumeral joint reaction force and the forces of 11 muscles, which were estimated through inverse dynamic analyses using the musculoskeletal model of the upper limb developed by Quental et al.[25,27] The muscle and joint reaction forces were applied at different attachment points, defined according to the anatomic coordinates of the musculoskeletal model of the upper limb applied, whose data are also based on the Visible Human Male data set.[36] Even though an attachment point does not belong to any mesh, it is able to transmit force to a set of nodes through the definition of coupling constraints. Muscle forces at the muscle attachment sites were distributed over a set of surface nodes closest to the corresponding attachment point. Forces due to the wrapping of muscles over anatomic structures were distributed over the nodes of the humeral surface closest to the projection of the force onto it. A similar approach was followed for the glenohumeral joint reaction force considering its application at the joint center. To avoid high punctual stresses, each attachment point was coupled with at least 30 nodes.[26,29] Figure 2 illustrates the surface nodes of the humerus for which coupling constraints were defined for the application of forces. To prevent rigid body motion, the base of the humerus was constrained in all directions.

Validation of bone remodeling model

Before the bone adaptation due to the stemless implants was studied, the intact bone model was used to qualitatively validate the application of the bone remodeling model based on its capacity to reproduce the actual bone density distribution of the humerus under analysis.[26,33,34] For this purpose, bone remodeling simulations were performed for different remodeling parameters κ and m, ranging between 1×10^{-5} and 3.5×10^{-4} and between 1 and 5, respectively, to find the set of parameters that best represented the intact humerus. All simulations were run for 200 iterations to allow bone to reach an equilibrium condition.[34,37] The actual bone density distribution of the humerus was estimated from the computed tomography (CT) images used to generate the 3D geometric model through the application of the Abaqus plug-in "bonemapy" (version 0.4.1, 2013)[19] and the calibration procedure described by Gupta and Dan.[12]

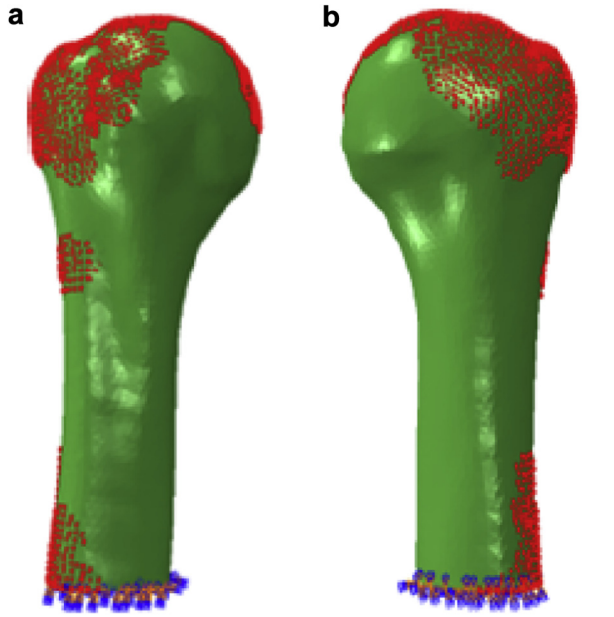

Figure 2 Three-dimensional finite element model of intact humerus: anterior view **(a)** and posterior view **(b)**. The nodes in *red* represent nodes on which muscle and joint reaction forces are applied.

To evaluate the bone density distributions obtained computationally, a statistical analysis was performed. The root-mean-square error (RMSE), based on relative ($_r\Delta\mu$) and absolute ($_a\Delta\mu$) differences, and the mean error (ME) between the predicted bone densities and those from the CT scan images were computed for each simulation. The mean and standard deviation of the bone density distributions were also evaluated. Because the humeral head is the most important region in this study, these measurements were only computed proximally until the surgical neck.[33] In addition, the surface of the humerus was excluded from the analyses to avoid considering bone densities computed from the CT images that were likely inaccurate owing to the partial volume effect.

Bone remodeling after shoulder arthroplasty

The bone remodeling simulations after shoulder arthroplasty were run for 200 iterations considering the bone remodeling parameters κ and m deemed the best to reproduce the actual bone density distribution of the humerus under analysis. The initial condition was defined as the final bone density distribution obtained for the intact bone model.

To evaluate the bone adaptation process of the humerus, qualitative and quantitative analyses were performed between the bone density distributions predicted for the intact bone model and the implanted models. Figure 3 summarizes the methodology adopted for the comparison of the results. For the qualitative analysis, absolute changes in bone density between the intact bone model and implanted models were visually assessed. For a quantitative assessment of the results, changes in bone mass for 16 proximal regions of the humerus were computed. Bone was divided into anterior, posterior, medial, and lateral regions of

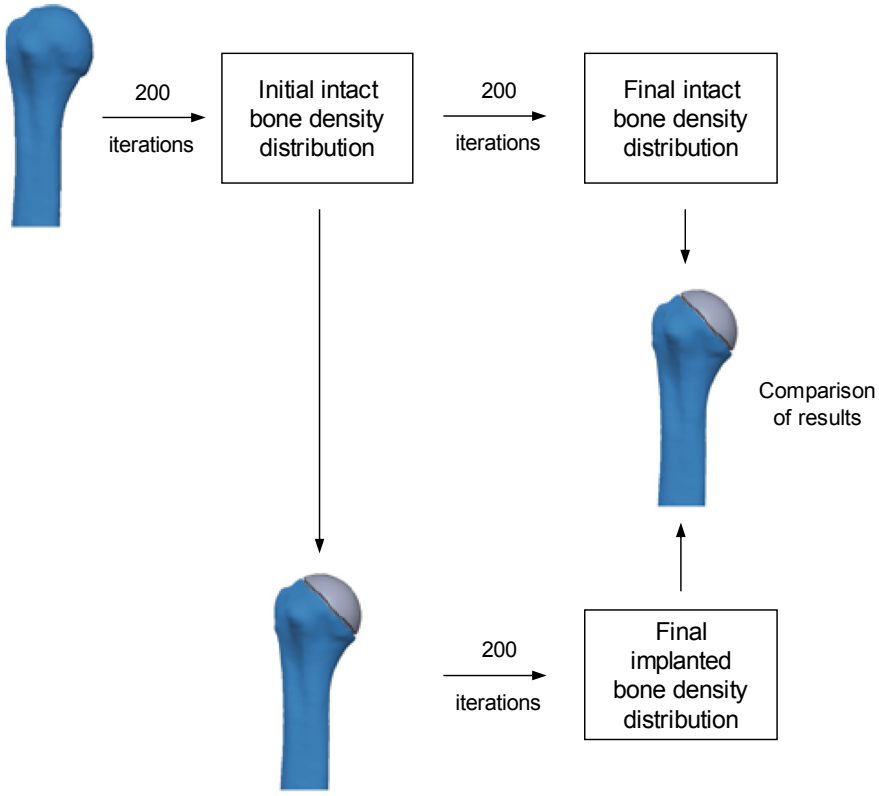

Figure 3 Methodology followed to evaluate bone adaptation process of humerus after shoulder arthroplasty.

interest (ROIs), and each of these regions was divided into proximal, distal, interior, and exterior, based on the studies of Alidousti et al[1] and Reeves et al,[32] as depicted in Figure 4. The change in bone mass (Δbm) was computed as follows:

$$\Delta bm(\%) = \frac{\sum_{i=1}^{n}\left(\mu_i^{Implanted} - \mu_i^{Intact}\right) \times V_i}{\sum_{i=1}^{n}\mu_i^{Intact} \times V_i} \times 100 \quad (3)$$

in which n is the total number of nodes within the ROI under analysis; V_i is the volume associated with node i; and $\mu_i^{Implanted}$ and μ_i^{Intact} are the bone densities of node i for the implanted and intact bone models, respectively.

Considering that the preservation of bone stock varies owing to the variability in design of the stemless implants considered in this study, an additional analysis was performed to evaluate the overall change in bone mass not only due to the bone adaptation process but also due to the surgical procedure. The reference mass was the bone mass of the intact humerus before shoulder arthroplasty.

Results

Validation of bone remodeling model

For all sets of parameters evaluated, the average change in bone density between consecutive iterations was smaller than 0.001 g · cm^{-3} at the end of the computational simulations. The RMSE and ME between the bone densities of the computational simulations and the CT scan images, as well as the mean and standard deviation of the density distributions, are detailed in Table II. For the sake of comparison, the RMSEs were normalized by the maximum RMSE obtained for each difference and the MEs were normalized by the mean density distribution of the CT scan images. Because the results for a parameter m of 4 and 5 were generally worse, only the results for 1, 2, and 3 are presented for conciseness.

The lowest RMSEs were obtained for parameters κ and m of 1.5×10^{-4} and 2, respectively, for the absolute difference and 2.5×10^{-4} and 2, respectively, for the relative difference. Because the solution obtained with a parameter κ of 1.5×10^{-4} presented the lowest ME, that is, the mean density distribution was closer to the actual density distribution of the humerus under analysis of 0.52 g · cm^{-3}, this parameter was deemed the best. Figure 5 presents the bone density distribution obtained for the best computational simulation and the CT scan images. For the sake of briefness, only 3 slices are shown.

Bone remodeling after shoulder arthroplasty

For all implanted models, the average change in bone density between consecutive iterations was smaller than 0.001 g · cm^{-3} at the end of the computational simulations. Figure 6 presents the absolute changes in bone density for each implanted bone with respect to the intact bone considering a fully completed condition of

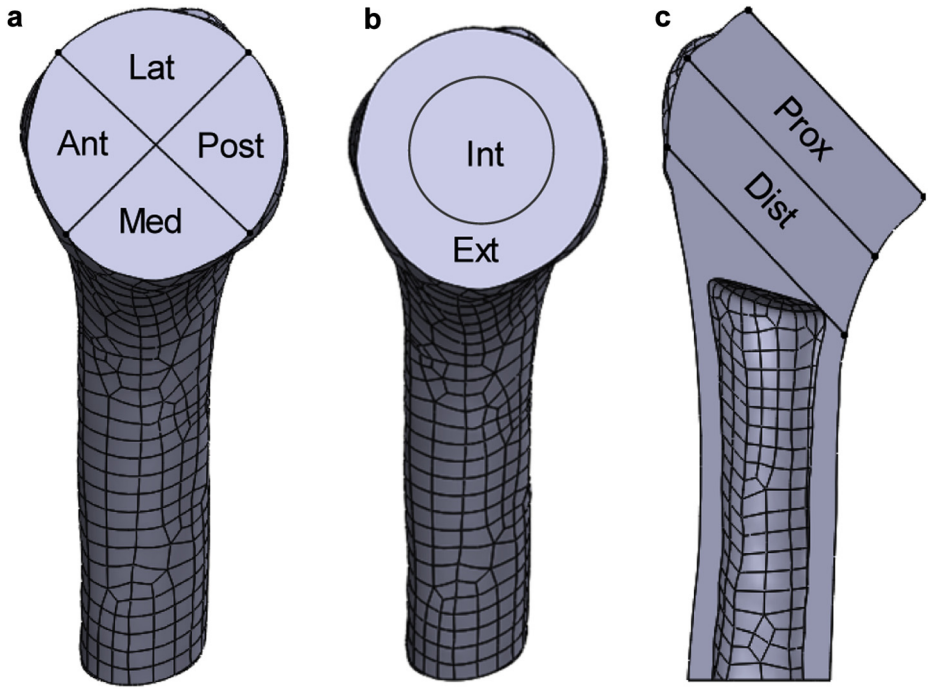

Figure 4 Regions of interest of humerus: medial views of resected surface **(a, b)** and anterior view of longitudinal cut **(c)**. *Lat*, lateral; *Ant*, anterior; *Post*, posterior; *Med*, medial; *Int*, interior; *Ext*, exterior; *Prox*, proximal; *Dist*, distal.

osseointegration. For the sake of simplicity, changes in bone density were categorized into equilibrium, for absolute changes between -0.1 and $0.1\ g \cdot cm^{-3}$, as well as 2 levels of bone resorption and bone apposition. Figure 7 presents in detail the changes in bone mass for the 16 ROIs of the humerus.

Overall, bone resorption was more pronounced in the proximal ROIs. The Eclipse-based implant led to the largest bone loss, whereas the SMR-based implant led to the least bone loss. The Eclipse-based, Global Icon–based, and Simpliciti-based implants showed bone resorption underneath the solid collar. The Sidus-based implant showed bone loss proximally, in the anteromedial region of the resected humerus. The simulation of contact between the humeral head and the resected surface of bone was predicted to have a negative impact on bone remodeling, especially for the Simpliciti- and Sidus-based stemless implants, which showed a substantial increase in bone loss in all proximal and interior ROIs. Bone apposition was mainly observed at the tip of the fins of all implants; at the interfaces between the resected surface of the humerus and the humeral heads of the SMR-, Simpliciti-, and Sidus-based implants when contact was simulated; and on the edge of the solid collar of the Simpliciti-based implant when no contact between the humeral head and bone was simulated.

The overall bone mass remaining in the humeral head after the surgical procedure, as well as the corresponding bone adaptation to the implant, is presented in Table III. The Eclipse-based implant was the design that preserved more bone stock during the shoulder arthroplasty. However, owing to the bone adaptation, it ended up losing its initial lead regarding bone stock as a result of being the design that caused the largest bone mass loss. Even though the SMR-based implant was the design that removed more bone during surgery, the impact on the bone adaptation process was the most positive.

Regarding the fully absent condition of osseointegration, no relevant qualitative differences were observed with respect to the fully completed condition in the simulations performed. For this reason and for the sake of briefness, the results for this condition are presented in Supplementary Figure S1 and Supplementary Table S1. Quantitatively, there was a general increase in bone apposition and a decrease in bone resorption.

Discussion

The objective of this study was to evaluate the influence of the variability in stemless designs on the bone adaptation process of the humerus. For this purpose, bone remodeling simulations were performed for 3D finite element models of 5 stemless designs based on implants available on the market. To qualitatively validate the application of the bone remodeling model to the humerus, the bone remodeling parameters that best reproduced the actual bone density distribution of the humerus under analysis were selected. The differences computed between the predicted bone densities and those from the CT scan images were small, and they were comparable to those reported in previous studies, which provides confidence in the results.[33,34] The performance of the stemless implants was evaluated by comparing the changes in bone density and bone mass

Table II Normalized RMSEs, based on relative and absolute differences, and MEs between bone densities of bone remodeling simulations and CT data, as well as mean bone density values

m	κ	RMSE		ME	Mean bone density (SD), g · cm^{-3}
		${}_a\Delta\mu$	${}_r\Delta\mu$		
1	1.0×10^{-5}	0.84	0.88	0.46	0.76 (0.37)
	5.0×10^{-5}	0.67	0.67	0.23	0.64 (0.37)
	1.0×10^{-4}	0.62	0.64	0.01	0.51 (0.36)
	1.5×10^{-4}	0.69	0.72	0.20	0.42 (0.35)
	2.0×10^{-4}	0.78	0.82	0.34	0.34 (0.34)
	2.5×10^{-4}	0.87	0.90	0.44	0.29 (0.32)
	3.0×10^{-4}	0.94	0.96	0.51	0.25 (0.31)
	3.5×10^{-4}	1.00	1.00	0.57	0.22 (0.30)
2	1.0×10^{-5}	0.84	0.90	0.48	0.76 (0.36)
	5.0×10^{-5}	0.66	0.67	0.23	0.64 (0.37)
	1.0×10^{-4}	0.56	0.61	0.11	0.58 (0.28)
	1.5×10^{-4}	0.54	0.55	0.01	0.51 (0.26)
	2.0×10^{-4}	0.56	0.53	0.10	0.47 (0.24)
	2.5×10^{-4}	0.58	0.53	0.17	0.43 (0.22)
	3.0×10^{-4}	0.61	0.54	0.22	0.41 (0.21)
	3.5×10^{-4}	0.63	0.54	0.26	0.38 (0.20)
3	1.0×10^{-5}	0.86	0.92	0.49	0.77 (0.35)
	5.0×10^{-5}	0.72	0.82	0.36	0.70 (0.31)
	1.0×10^{-4}	0.63	0.74	0.23	0.64 (0.27)
	1.5×10^{-4}	0.59	0.71	0.15	0.60 (0.24)
	2.0×10^{-4}	0.57	0.69	0.09	0.57 (0.22)
	2.5×10^{-4}	0.57	0.67	0.05	0.54 (0.21)
	3.0×10^{-4}	0.56	0.66	0.01	0.53 (0.20)
	3.5×10^{-4}	0.56	0.65	0.01	0.51 (0.19)

RMSE, root-mean-square error; ${}_r\Delta\mu$, relative difference; ${}_a\Delta\rho$, absolute difference; *ME*, mean error; *CT*, computed tomography; *SD*, standard deviation.
The RMSEs presented for ${}_r\Delta\mu$ and ${}_a\Delta\rho$ were normalized by the maximum RMSE computed for each difference, that is, 0.78 and 0.38 g · cm^{-3}, respectively. The MEs were normalized by the mean density distribution of the CT scan images, that is, 0.52 g · cm^{-3}.

between the implanted bone models and the intact bone model. The amount of bone removed during the surgical procedure was also assessed for all implants.

The results showed that the implant designs impact not only the bone adaptation process but also the amount of bone remaining immediately after shoulder arthroplasty. The implant that preserved more bone during implantation was the Eclipse-based model, whereas the implant that removed more bone was the SMR-based model, which only preserved about 50% of the intact humeral head mass. Despite the Eclipse-based implant preserving more bone stock, its impact on the bone adaptation process of the humerus was the most negative. Bone resorption was particularly pronounced proximally in the interior, lateral, and anterior ROIs, as also observed clinically by Habermeyer et al,[13] Hawi et al,[15] and Heuberer et al[18] through radiologic assessment. Considering the observation of radiolucent lines beneath the baseplate of the Eclipse

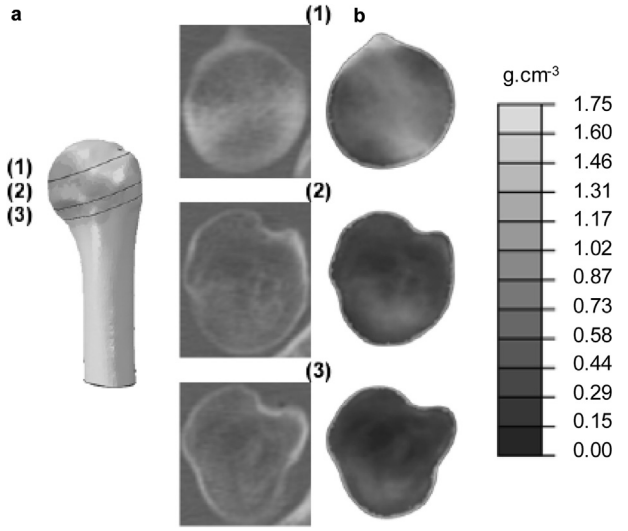

Figure 5 Bone density distribution for 3 slices of humerus: computed tomography scan images **(a)** and computational simulation deemed best **(b)**.

implant, Gallacher et al[9] suggested the occurrence of stress shielding caused by the preferential transfer of loads through the central screw, which was confirmed by the bone remodeling simulations performed in our study. Compared with the remaining implants, the Eclipse-based design has the longest central structure, which may have contributed to its poorer performance as loads are mainly transferred through the central screw and thus are only transmitted to the bone at more distal regions. An interesting finding was that even though the SMR-based model removed the largest amount of bone during shoulder arthroplasty, its impact on the bone adaptation process of the humerus was the most positive. When the implant was placed according to the surgical technique, that is, with the humeral head contacting the bone surface, the overall change in bone mass was negligible, and when the humeral head component was not put into contact with the bone surface, the bone mass increased by 15.2%. Two implantation features may have contributed to this positive outcome of the SMR-based implant. On the one hand, during its implantation, bone is removed from the most interior region of the humeral head, where most implants presented bone loss. On the other hand, the SMR-based implant is fixed proximally in a more peripheral, stronger region of the humerus,[1] which likely allows a more natural transmission of loads from the humeral head component to the remaining bone. For the Global Icon–based, Simpliciti-based, and Sidus-based implants, the results were similar when the contact between the humeral heads and bone was disregarded. When contact existed for the Simpliciti- and Sidus-based implants, bone resorption increased substantially in the most proximal and interior ROIs because loads transferred previously through the metaphyseal fixation features started also to be transferred through contact in more peripheral regions. This result suggests that avoiding contact between the humeral

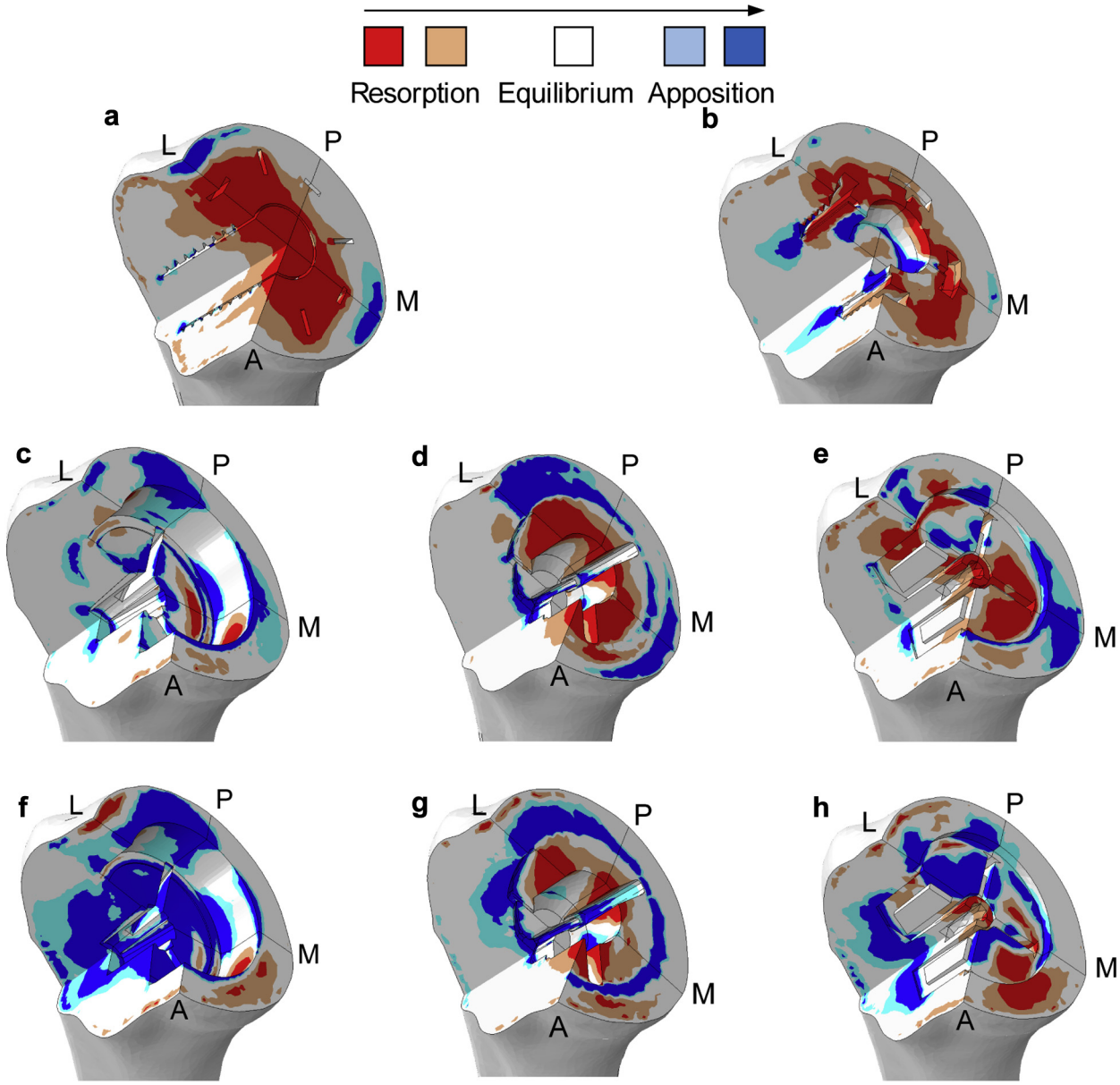

Figure 6 Absolute changes in bone density ($\Delta\mu$) between implanted models and the intact bone model for the fully completed condition of osseointegration for Eclipse-based **(a)**, Global Icon–based **(b)**, SMR-based **(c, f)**, Simpliciti-based **(d, g)**, and Sidus-based **(e, h)** stemless implants. The results in **c**, **d**, and **e** were obtained considering contact between the humeral heads of the implants and the resected surface of bone, whereas the results in **f**, **g**, and **h** were obtained considering no contact. Bone resorption is depicted in *red* ($\Delta\mu < -0.2$ g · cm^{-3}) and *orange* (-0.2 g · cm$^{-3} < \Delta\mu < -0.1$ g · cm^{-3}), whereas bone apposition is depicted in *light blue* (0.1 g · cm$^{-3} < \Delta\mu < 0.2$ g · cm^{-3}) and *dark blue* ($\Delta\mu > 0.2$ g · cm^{-3}). *White* denotes an equilibrium condition (-0.1 g · cm$^{-3} < \Delta\mu < 0.1$ g · cm^{-3}). *L*, lateral; *P*, posterior; *M*, medial; *A*, anterior.

heads of the stemless implants and the resected surface of the humerus provides a better outcome from the bone adaptation point of view. For the Sidus-based model, bone loss was observed proximally, especially in the lateral and anterior ROIs, which is consistent with the radiologic findings of Krukenberg et al.[20]

Among the 5 stemless designs that we studied, 3 possess a solid collar, namely the Eclipse-based, Global Icon–based, and Simpliciti-based models. For these implants, bone resorption occurred in the proximal interior region of the resected humerus covered by the collar, as also observed in previous midterm radiologic studies on the Eclipse implant.[13,18] Churchill and Athwal[2] suggested that in the case of stress shielding and bone resorption occurring, collared implants could provide more stability than collarless implants. However, because the bone resorption observed under the collar could contribute to implant loosening, further research is necessary to assess the effective contribution of the collar to the long-term stability of stemless implants.

ROI			Eclipse-based		Global Icon-based		Humeral head contacts bone						Humeral head does not contact bone					
							SMR-based		Simpliciti-based		Sidus-based		SMR-based		Simpliciti-based		Sidus-based	
Prox	Int	Lat	-42.9	-34.1	0.2	-2.6	-	-	-32.7	-25.5	-35.5	-28.6	-	-	-2.4	-4.1	-10.1	-4.6
		Post	-14.5		-14.1		-		-19.8		-13.1		-		-5.5		7.9	
		Med	-31.3		1.3		-		-13.8		-32.7		-		7.7		-5.1	
		Ant	-38.9		1.2		-		-35.6		-36.1		-		-16.7		-15.1	
	Ext	Lat	-13.8	-11.9	-3.7	-8.0	-4.8	-2.7	-1.2	-3.3	-13.1	-7.5	1.9	1.9	9.1	1.7	2.1	-2.4
		Post	-5.1		-5.1		10.1		1.7		2.7		19.1		3.6		11.0	
		Med	-4.2		-11.1		-1.8		-2.7		-1.6		-5.4		-4.8		-11.2	
		Ant	-23.5		-13.1		-10.1		-12.1		-18.7		-1.8		-1.3		-10.0	
Dist	Int	Lat	-6.9	-5.8	24.4	15.5	10.5	9.7	9.3	5.2	-3.2	1.2	83.2	68.8	49.9	27.1	47.0	32.6
		Post	9.5		-1.2		15.1		16.3		13.0		69.9		25.1		32.3	
		Med	1.4		-1.2		15.2		6.9		-2.6		102.2		20.5		13.5	
		Ant	-15.5		29.4		4.4		-6.1		-3.3		44.1		15.6		36.9	
	Ext	Lat	-9.3	-9.3	12.3	1.9	-1.5	-2.1	-2.2	-1.4	-9.2	-3.6	16.3	7.0	14.1	4.7	15.1	7.7
		Post	-1.9		-4.7		3.3		3.1		5.1		10.0		0.0		8.8	
		Med	-6.4		1.1		-2.4		0.6		0.5		10.9		6.7		8.8	
		Ant	-21.1		-3.1		-5.8		-6.7		-14.2		-11.6		-6.0		-5.7	
	Total		-13.8		-1.8		0.7		-4.1		-7.8		15.2		4.5		4.0	

Figure 7 Changes in bone mass, as percentages, for 16 regions of interest (*ROIs*) of humerus with respect to the intact bone model for the fully completed condition of osseointegration. A 3-color scale is used to highlight the changes. The ROIs that present the largest bone resorption and bone apposition are *dark red* and *dark blue*, respectively, and the ROIs that show the median change in bone mass are *white*. All remaining ROIs are colored proportionally. *Lat*, lateral; *Post*, posterior; *Int*, interior; *Med*, medial; *Ant*, anterior; *Prox*, proximal; *Ext*, exterior; *Dist*, distal.

Table III Bone mass in humeral head

	Bone mass, %							
	Eclipse based	Global Icon based	Humeral head contacts bone			Humeral head does not contact bone		
			SMR based	Simpliciti based	Sidus based	SMR based	Simpliciti based	Sidus based
Intact model condition	100	100	100	100	100	100	100	100
After surgical procedure	64	62	51	61	61	51	61	61
After corresponding bone adaptation to implant	55	60	51	59	56	59	64	63

Bone mass in the humeral head is presented as a percentage of the bone mass in the intact model after the surgical procedure and the corresponding bone adaptation to the implant for the fully completed condition of osseointegration.

For the fully absent condition of osseointegration, a general increase in bone apposition and a decrease in bone resorption were observed, but the qualitative findings observed for the fully completed condition remained as the relative performance of the 5 stemless designs studied was not affected.

To our knowledge, no other studies have addressed the effect of the geometry of different stemless implants on the bone adaptation process of the humerus. Reeves et al[32] studied the effect of the fixation design of generic stemless implants on bone stress and strain responses. Although a potential bone response was defined based on strain energy density changes, the actual process of bone adaptation was not simulated, as opposed to our study. Furthermore, in addition to having considered only 2 loading conditions, Reeves et al considered no muscle forces, which conditions the simulation of the mechanical environment of the humerus, as reported by Quental et al.[28] Using the bone remodeling model applied in our study, Santos et al[33] studied the bone adaptation process of the humerus after the implantation of a resurfacing implant and a stemless implant based on the Sidus Stem-Free Shoulder System. Considering only the Sidus-based model in which the humeral head contacted the bone for

the sake of comparison, our results are consistent with those presented by Santos et al, that is, bone resorption occurred mainly proximally, especially in the lateral and anterior ROIs, and bone apposition occurred in the distal posterior ROI. It should be noted that a direct quantitative comparison of the results is difficult because of the different definitions of the ROIs. Moreover, the procedure followed for the application of the loading conditions was different than that followed in our study, which impacted the bone adaptation results. This study considered forces not only due to the pulling of muscles at the attachment sites but also due to the wrapping of muscles over anatomic structures, whereas Santos et al considered only the forces at the muscle attachment sites.

Despite this study providing further insight into the behavior of stemless implants, its findings must be interpreted bearing in mind that only bone adaptation was evaluated. Because the complications of shoulder arthroplasty often have a multifactorial etiology,[7] other biomechanical aspects, such as short- and long-term stability, must also be considered to allow definite recommendations. Regarding the placement of the humeral head implant, the bone remodeling simulations performed suggest that contact should not exist between the implant and the resected surface of bone. When studying the primary stability of the Sidus Stem-Free Shoulder System during upper-limb activities, Favre and Henderson[6] reported that the micromotions estimated computationally were smaller than the generally accepted threshold of 150 μm below which bone ingrowth occurs, even though the interaction between the humeral head implant and bone was not considered, which provides confidence in the primary stability of the implant without the humeral head contacting the bone. Nevertheless, further investigation on the contribution of the humeral head contact to the short- and long-term stability of the implant is necessary to support definite recommendations. In addition, several limitations of this study must be considered. Even though the results are expected to be representative of humeri in general as the dimensions of the humerus analyzed fall within those of typical humeri,[17] only the geometry of 1 right humerus was considered. Two extreme conditions of full or no osseointegration were considered to evaluate the impact of the interaction conditions on the bone adaptation process, but the osseointegration process was not effectively simulated. As in other computational studies of bone adaptation,[26,33,34] the application of the bone remodeling model was validated considering its ability to reproduce the actual bone density distribution of the humerus. Nonetheless, a sensitivity analysis on parameter k, in which the bone remodeling simulations were repeated for parameters k 50% larger and 50% smaller than that deemed the best, showed no relevant impact on the findings of this study, which provides further confidence in the results. The 3D geometric models of the stemless implants studied were not provided by the manufacturers. Consequently, the stemless designs considered in this study approximate the implants available on the market.

Conclusion

Considering 3D finite element models, the aim of this study was to investigate the influence of 5 stemless designs on the bone adaptation process of the humerus. Overall, the bone adaptation results showed that the geometry of the stemless implants influences the bone adaptation process of the humerus, supporting that the extrapolation of findings from 1 specific design to all stemless designs is not appropriate. From the bone adaptation point of view, the Eclipse-based model presented the worst performance whereas the SMR-based model presented the best. Furthermore, contact between the humeral head implant and the resected bone surface was seen to be harmful to the bone adaptation process. Despite our study providing further insight into the behavior of stemless implants, its findings must be interpreted with caution as additional factors, other than bone adaptation, must be considered to allow definite recommendations. To our knowledge, this is the first study to perform such an extensive evaluation of the impact of different stemless implants, available for use, on the bone adaptation process of the humerus.

Disclaimer

This work was supported by the Portuguese Foundation for Science and Technology (FCT), through IDMEC, under LAETA (project UID/EMS/50022/2019).

The authors, their immediate families, and any research foundations with which they are affiliated have not received any financial payments or other benefits from any commercial entity related to the subject of this article.

Supplementary data

Supplementary data to this article can be found online at https://doi.org/10.1016/j.jse.2019.03.007.

References

1. Alidousti H, Giles JW, Emery RJH, Jeffers J. Spatial mapping of humeral head bone density. J Shoulder Elbow Surg 2017;26:1653-61. https://doi.org/10.1016/j.jse.2017.03.006
2. Churchill RS, Athwal GS. Stemless shoulder arthroplasty—current results and designs. Curr Rev Musculoskelet Med 2016;9:10-6. https://doi.org/10.1007/s12178-016-9320-4

3. Coley B, Jolles BM, Farron A, Aminian K. Detection of the movement of the humerus during daily activity. Med Biol Eng Comput 2009;47:467-74. https://doi.org/10.1007/s11517-009-0464-x
4. Coley B, Jolles BM, Farron A, Aminian K. Arm position during daily activity. Gait Posture 2008;28:581-7. https://doi.org/10.1016/j.gaitpost.2008.04.014
5. Eberle S, Augat P. Preventing contact convergence problems in bone–implant contact models. In: ANSYS Conference, 25th CADFEM Users Meeting. Grafing bei München: CADFEM GmbH; 2007. p. 21-5.
6. Favre P, Henderson AD. Prediction of stemless humeral implant micromotion during upper limb activities. Clin Biomech 2016;36:46-51. https://doi.org/10.1016/j.clinbiomech.2016.05.003
7. Fealy S, Sperling JW, Warren RF, Craig EV. Shoulder arthroplasty: complex issues in the primary and revision setting. New York: Thieme Medical Publishers; 2008.
8. Fernandes P, Rodrigues H, Jacobs C. A model of bone adaptation using a global optimisation criterion based on the trajectorial theory of Wolff. Comput Methods Biomech Biomed Engin 1999;2:125-38.
9. Gallacher S, Williams HLM, King A, Kitson J, Smith CD, Thomas WJ. Clinical and radiologic outcomes following total shoulder arthroplasty using Arthrex Eclipse stemless humeral component with minimum 2 years' follow-up. J Shoulder Elbow Surg 2018;27:2191-7. https://doi.org/10.1016/j.jse.2018.05.039
10. Grant JA, Bishop NE, Gotzen N, Sprecher C, Honl M, Morlock MM. Artificial composite bone as a model of human trabecular bone: the implant-bone interface. J Biomech 2007;40:1158-64. https://doi.org/10.1016/j.jbiomech.2006.04.007
11. Guedes JM, Kikuchi N. Preprocessing and postprocessing for materials based on the homogenization method with adaptive finite element methods. Comput Methods Appl Mech Eng 1990;83:143-98.
12. Gupta S, Dan P. Bone geometry and mechanical properties of the human scapula using computed tomography data. Trends Biomater Artif Organs 2004;17:61-70.
13. Habermeyer P, Lichtenberg S, Tauber M, Magosch P. Midterm results of stemless shoulder arthroplasty: a prospective study. J Shoulder Elbow Surg 2015;24:1463-72. https://doi.org/10.1016/j.jse.2015.02.023
14. Haider IT, Speirs AD, Beaulé PE, Frei H. Influence of ingrowth regions on bone remodeling around a cementless hip resurfacing femoral implant. Comput Methods Biomech Biomed Engin 2015;18:1349-57. https://doi.org/10.1080/10255842.2014.903931
15. Hawi N, Magosch P, Tauber M, Lichtenberg S, Habermeyer P. Nine-year outcome after anatomic stemless shoulder prosthesis: clinical and radiologic results. J Shoulder Elbow Surg 2017;26:1609-15. https://doi.org/10.1016/j.jse.2017.02.017
16. Hawi N, Tauber M, Messina MJ, Habermeyer P, Martetschlager F. Anatomic stemless shoulder arthroplasty and related outcomes: a systematic review. BMC Musculoskelet Disord 2016;17:376. http://doi.org/10.1186/s12891-016-1235-0
17. Hertel R, Knothe U, Ballmer FT. Geometry of the proximal humerus and implications for prosthetic design. J Shoulder Elbow Surg 2002;11:331-8. https://doi.org/10.1067/mse.2002.124429
18. Heuberer PR, Brandl G, Pauzenberger L, Laky B, Kriegleder B, Anderl W. Radiological changes do not influence clinical mid-term outcome in stemless humeral head replacements with hollow screw fixation: a prospective radiological and clinical evaluation. BMC Musculoskelet Disord 2018;19:28. https://doi.org/10.1186/s12891-018-1945-6
19. Hogg M. GitHub. Mhogg/Bonemapy: an Abaqus plug-in to map bone properties from CT scans to 3D finite element bone/implant models, https://github.com/mhogg/bonemapy; 2013, accessed March 19, 2018.
20. Krukenberg A, McBirnie J, Bartsch S, Böhler N, Wiedemann E, Jost B, et al. Sidus Stem-Free Shoulder System for a primary osteoarthritis: short-term results of a multicenter study. J Shoulder Elbow Surg 2018;27:1483-90. https://doi.org/10.1016/j.jse.2018.02.057
21. LimaCorporate. SMR stemless [brochure]. LimaCorporate: San Daniele del Friuli; 2016.
22. Lin DJ, Wong TT, Kazam JK. Shoulder arthroplasty, from indications to complications: what the radiologist needs to know. Radiographics 2016;36:192-208. https://doi.org/10.1148/rg.2016150055
23. Lübbeke A, Rees JL, Barea C, Combescure C, Carr AJ, Silman AJ. International variation in shoulder arthroplasty. Acta Orthop 2017;88:592-9. https://doi.org/10.1080/17453674.2017.1368884
24. Nagels J, Stokdijk M, Rozing PM. Stress shielding and bone resorption in shoulder arthroplasty. J Shoulder Elbow Surg 2003;12:35-9. https://doi.org/10.1067/mse.2003.22
25. Quental C, Azevedo M, Ambrósio J, Gonçalves SB, Folgado J. Influence of the musculotendon dynamics on the muscle force sharing problem of the shoulder—a fully inverse dynamics approach. J Biomech Eng 2018;140:071005. https://doi.org/10.1115/1.4039675
26. Quental C, Fernandes PR, Monteiro J, Folgado J. Bone remodelling of the scapula after a total shoulder arthroplasty. Biomech Model Mechanobiol 2014;13:827-38. https://doi.org/10.1007/s10237-013-0537-5
27. Quental C, Folgado J, Ambrósio J, Monteiro J. Critical analysis of musculoskeletal modelling complexity in multibody biomechanical models of the upper limb. Comput Methods Biomech Biomed Engin 2015;18:749-59. https://doi.org/10.1080/10255842.2013.845879
28. Quental C, Folgado J, Fernandes PR, Monteiro J. Computational analysis of polyethylene wear in anatomical and reverse shoulder prostheses. Med Biol Eng Comput 2015;53:111-22. https://doi.org/10.1007/s11517-014-1221-3
29. Quental C, Folgado J, Fernandes PR, Monteiro J. Bone remodelling analysis of the humerus after a shoulder arthroplasty. Med Eng Phys 2012;34:1132-8. https://doi.org/10.1016/j.medengphy.2011.12.001
30. Rancourt D, Shirazi-Adl A, Drouin G, Paiement G. Friction properties of the interface between porous-surfaced metals and tibial cancellous bone. J Biomed Mater Res 1990;24:1503-19.
31. Razfar N, Reeves JM, Langohr DG, Willing R, Athwal GS, Johnson JA. Comparison of proximal humeral bone stresses between stemless, short stem, and standard stem length: a finite element analysis. J Shoulder Elbow Surg 2016;25:1076-83. https://dx.doi.org/10.1016/j.jse.2015.11.011
32. Reeves JM, Langohr GDG, Athwal GS, Johnson JA. The effect of stemless humeral component fixation feature design on bone stress and strain response: a finite element analysis. J Shoulder Elbow Surg 2018;27:2232-41. https://doi.org/10.1016/j.jse.2018.06.002
33. Santos B, Quental C, Folgado J, Sarmento M, Monteiro J. Bone remodelling of the humerus after a resurfacing and a stemless shoulder arthroplasty. Clin Biomech 2018;59:78-84. https://doi.org/10.1016/clinbiomech.2018.09.009
34. Sharma GB, Debski RE, McMahon PJ, Robertson DD. Adaptive glenoid bone remodeling simulation. J Biomech 2009;42:1460-8. https://doi.org/10.1016/j.jbiomech.2009.04.002
35. Sobocinski M. Analysis of biobearings friction and wear processes. J Appl Math Comput Mech 2015;14:103-9. https://doi.org/10.17512/jamcm.2015.2.11
36. Spitzer V, Ackerman MJ, Scherzinger AL, Whitlock D. The visible human male: a technical report. J Am Med Inform Assoc 1996;3:118-30.
37. Suárez DR, Weinans H, Van Keulen F. Bone remodeling around a cementless glenoid component. Biomech Model Mechanobiol 2012;11:903-13. https://doi.org/10.1007/s10237-011-0360-9
38. Yushkevich PA, Piven J, Hazlett HC, Smith RG, Ho S, Gee JC, et al. User-guided 3D active contour segmentation of anatomical structures: significantly improved efficiency and reliability. Neuroimage 2006;31:1116-28. https://doi.org/10.1016/j.neuroimage.2006.01.015